Support information for

Epitaxial Growth of Large-scale In_2S_3 Nanoflakes and the Construction of High Performance In_2S_3/Si Photodetector

Jianting Lu[1], Zhaoqiang Zheng[1, 2*], Wei Gao[1], Jiandong Yao[3], Yu Zhao[1], Ye Xiao[1], Bing Wang[4]

Jingbo Li[1, 5*]

[1] School of Materials and Energy, Guangdong University of Technology, Guangzhou, 510006, Guangdong, P. R. China.

[2] Department of Electronic Engineering, The Chinese University of Hong Kong, Hong Kong SAR, P. R. China.

[3] State Key Laboratory of Optoelectronic Materials and Technologies, Nanotechnology Research Center, School of Materials Science & Engineering, Sun Yat-sen University, Guangzhou, 510275, Guangdong, P. R. China.

[4] Institute of Micro-nano Optoelectronic Technology, Shenzhen Key Lab of Micro-nano Photonic Information Technology, College of Electronic Science and Technology, Shenzhen University, Shenzhen, 518060, Guangdong, P. R. China.

[5] State Key Laboratory for Superlattices and Microstructures, Institute of Semiconductors, Chinese Academy of Sciences, Beijing, 100083, P. R. China.

*Corresponding authors: zhengzhq5@mail2.sysu.edu.cn and jbli@semi.ac.cn

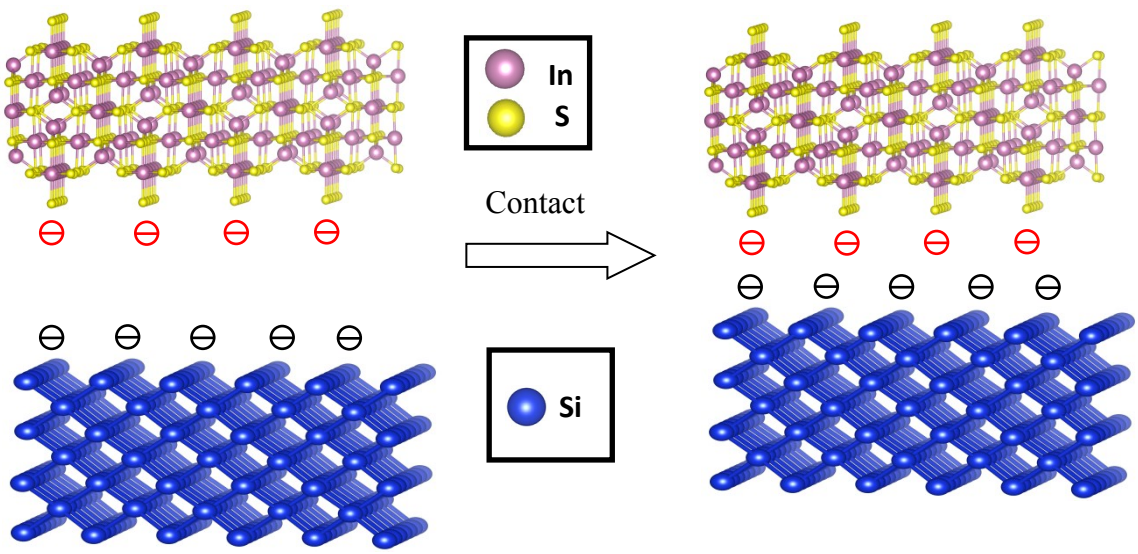

Figure S1. Compatibility between In_2S_3 and Si. Since both In_2S_3 and Si are non-layered structures, there are many unsaturated dangling bonds on the surface of S atoms and Si atoms, as shown on the left. After the transfer of In_2S_3 onto Si, since the electronegativity of the S atom is greater than that of the Si atom, the unsaturated dangling bonds on the surface Si atoms will be attracted to the surface of the S atoms, as shown on the right. Therefore, In_2S_3 and Si will be tightly packed together to form an excellent heterojunction.

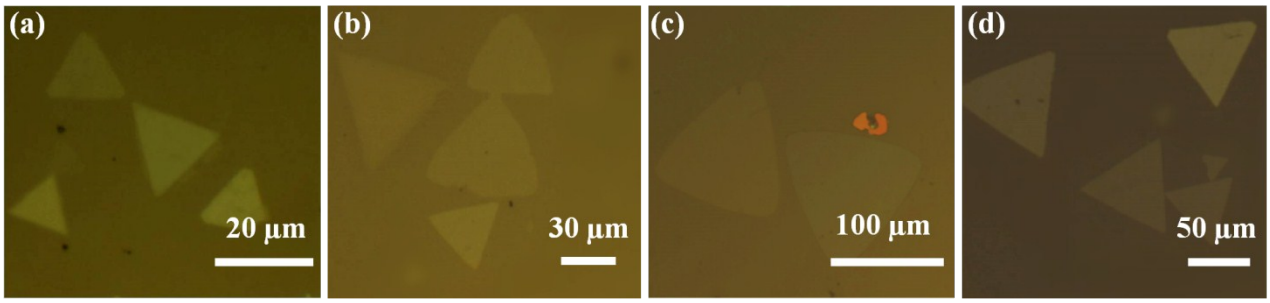

Figure S2. Optical images of the as-grown β-In_2S_3 flakes obtained at different temperatures: (a) 900 ℃. (b) 950 ℃. (c) 980 ℃. (d) 1020 ℃. As can be seen, we have prepared In_2S_3 nanoflakes under various temperatures. With the increase of the growth temperature, the size of the In_2S_3 nanoflakes increases. When the growth temperature increases to be more than 980 ℃, the size slightly declines. Therefore, 980 ℃ is chosen as the optimum growth temperature in this work.

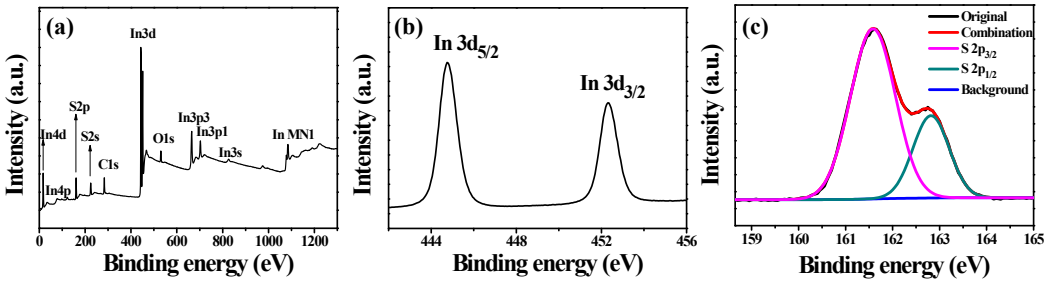

Figure S3. XPS pattern of In_2S_3. (a) Full spectrum of In_2S_3. Core spectrum of (b) In_{3d} and (c) S_{2p}.

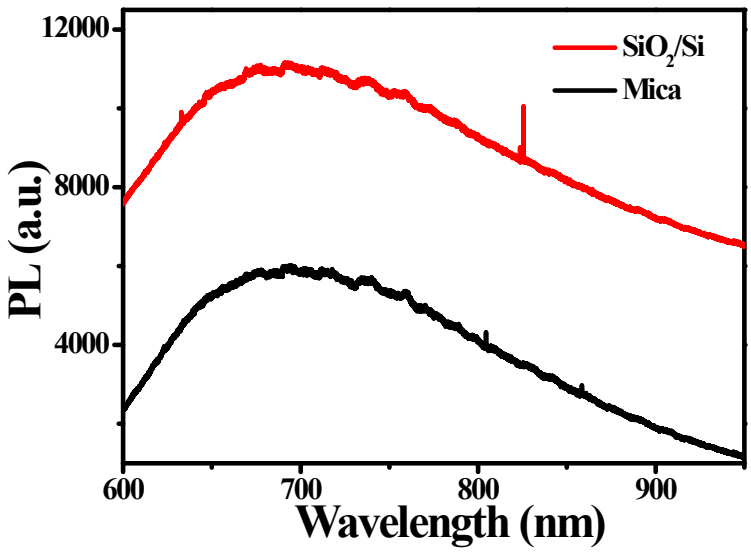

Figure S4. PL spectrum of original In_2S_3 on the mica substrate (before) and transferred In_2S_3 on SiO_2/Si substrate (after).

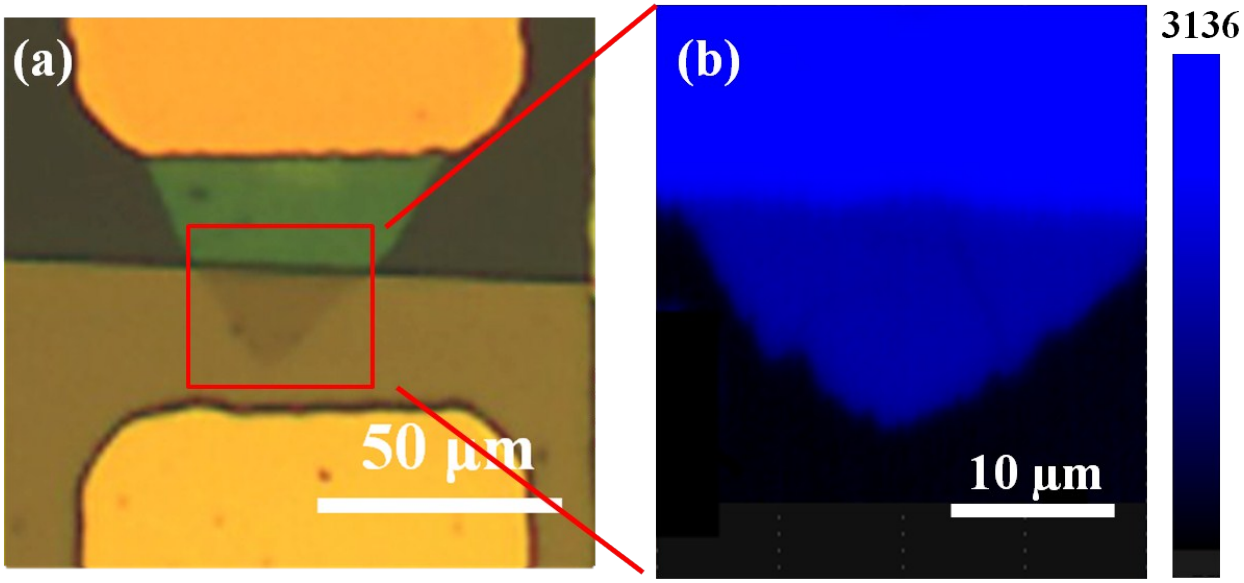

Figure S5. (a) Optical microscope image of the In_2S_3/Si device. (b) The PL mapping of the In_2S_3/Si device, corresponding to the red rectangle in (a). Recognizable PL quenching is observed at the In_2S_3/Si heterojunction.

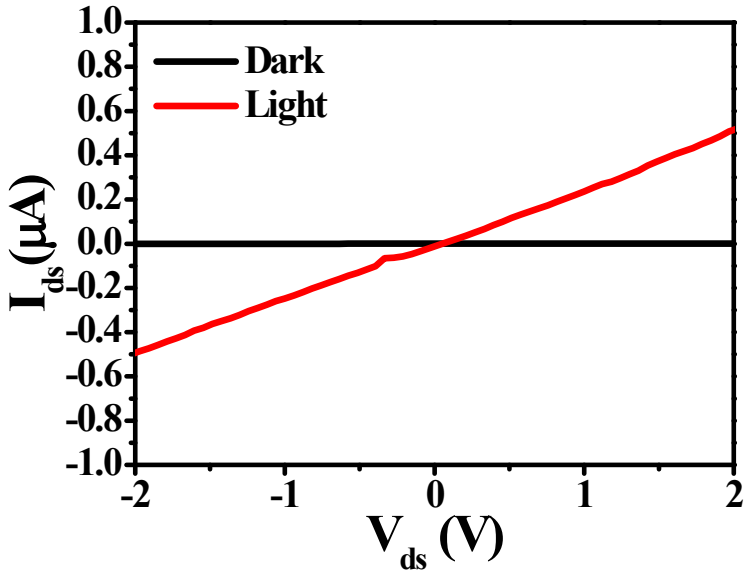

Figure S6. I_{ds}-V_{ds} curves of planar In_2S_3 device under dark and light illumination. The nearly linear I-V curves prove the good Ohmic-contacts for Ti/Au-In_2S_3.

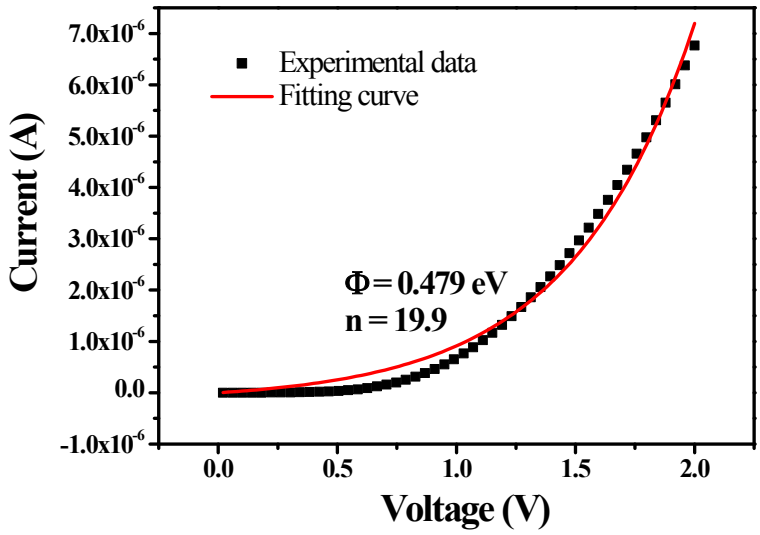

Figure S7. The fitting curve of barrier height of the In_2S_3/Si heterojunction by using the thermionic emission theory-based diode equation.

The current through a Schottky junction can be described by the well-known Richardson–Dushman thermionic emission theory[1-2]:

$$I = I_s[\exp\left(\frac{eV}{nkT}\right) - 1] \quad \textbf{(1)}$$

$$I_s = A_1 A^* T^2 exp(-\frac{e\emptyset_b}{kT}) \quad \textbf{(2)}$$

where I_S is the reverse saturation current, e is the electronic charge, V is the bias voltage, n is the ideality factor, k is the Boltzmann constant, T is the absolute temperature, A_1 is the area of the device, ϕ_b is the Schottky barrier height, and A* is the effective Richardson constant (32 A cm^{-2} K^{-2} for p-type Si). On the basis of the above equations, by fitting the dark I–V curves of these two devices, ϕ_b can be deduced to be 0.479 eV for the graphene/Si Schottky junction.

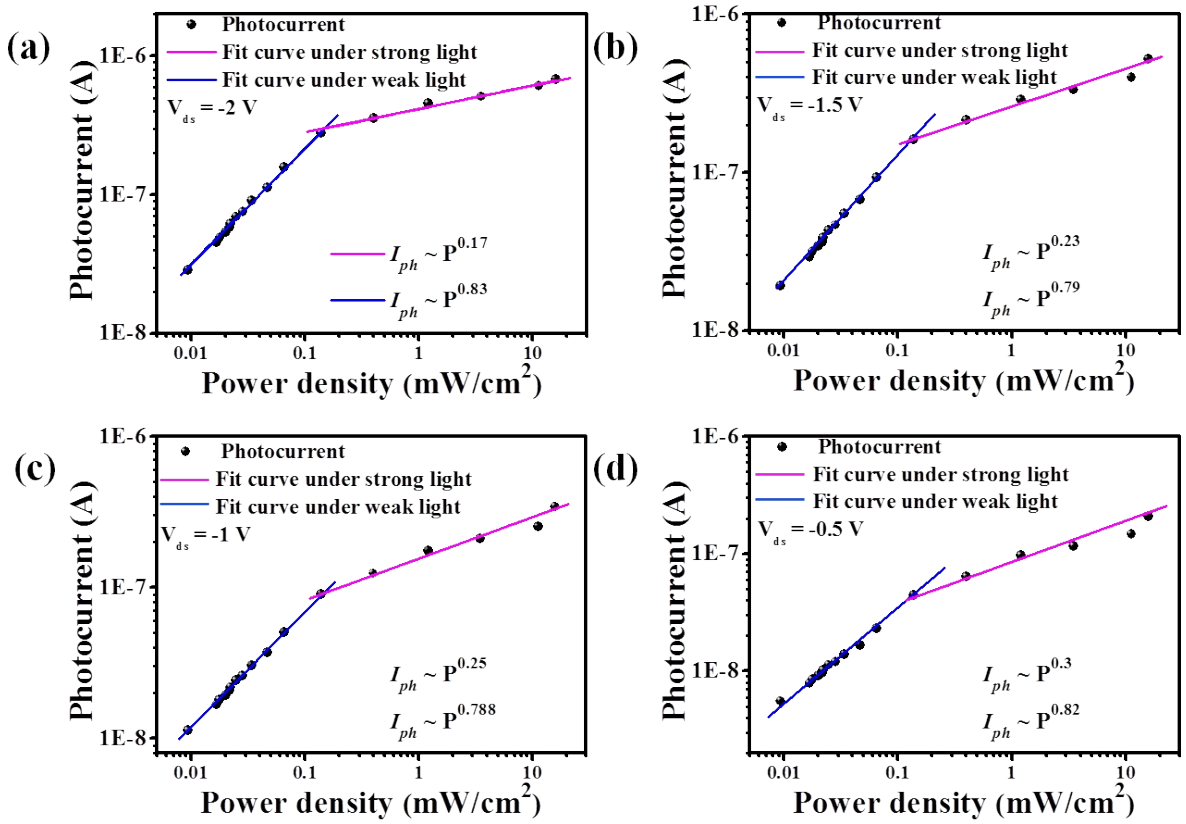

Figure S8. Photocurrent versus illumination power density at the applied voltage of (a) -2 V; (b) -1.5 V (c) -1 V (d) -0.5 V.

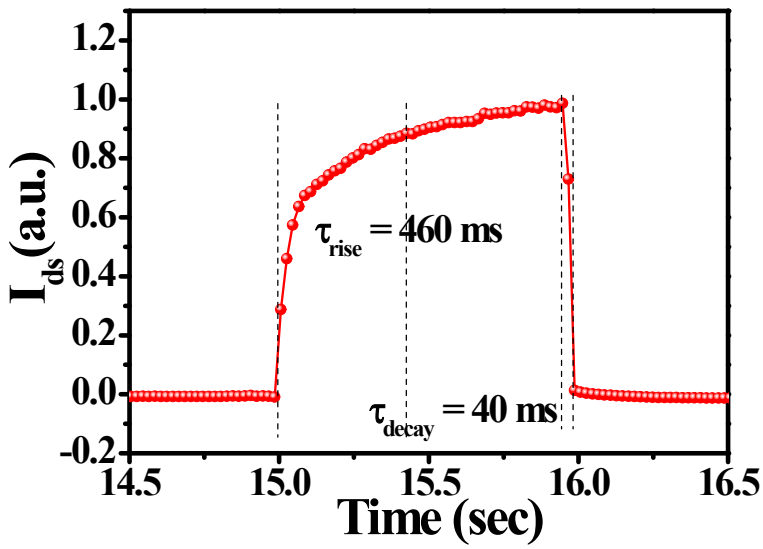

Figure S9. The magnified and normalized plot of one response cycle of pure In_2S_3 device.

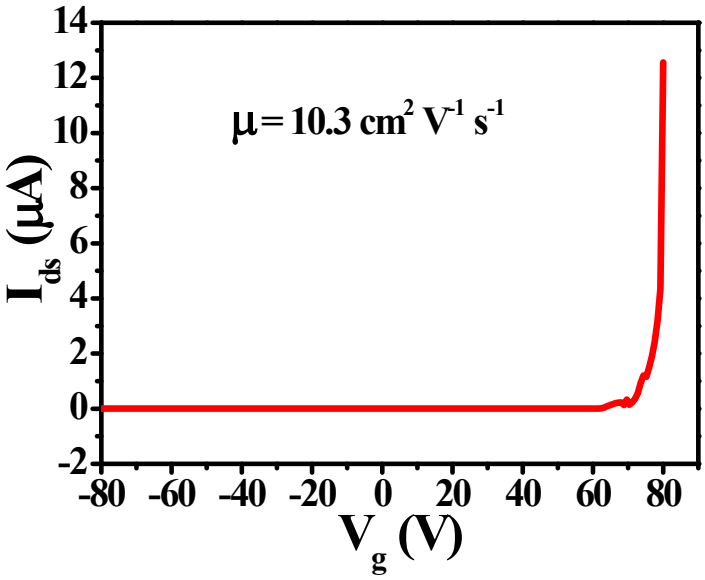

Figure S10. The transfer curve of planar In_2S_3 device.

The electron mobility can be acquired by the following equation[3-4]

$$\mu = \frac{\partial I_{ds}}{\partial V_g}\left(\frac{Ld}{W\varepsilon_o\varepsilon_r V_{ds}}\right)$$

where L and W are the length and width of the channel, $\frac{\partial I_{ds}}{\partial V_g}$ is slope of the transfer curve, μ is mobility, ε_r is the relative static permittivity, ε_0 is the electric constant, and d is the thickness of the SiO_2 layer. Herein, V_{ds} = 2 V, L = 14 μm, W = 22 μm, and d = 300 nm. Then, $\varepsilon_0 = 8.85 \times 10^{-12}$ F/m, $\varepsilon_r = 3.9$, and $\frac{\partial I_{ds}}{\partial V_g} = 4.58 \times 10^{-7}$ A/V. Based on the data above, the electron mobility is calculated to be 10.3 $cm^2\ V^{-1}\ s^{-1}$.

Table S1. Key parameters comparison between our In_2S_3/Si device and other non-layered 2D materials based photodetectors. Commercial Si device is also included.

Devices	Method	Lateral (μm)	R (A/W)	D* (Jones)	On/off ratio	Rise/decay time (ms)	Ref.
In_2S_3/Si	**PVE**	**~ 161**	**579.6**	**2.1×10^{11}**	**~ 552**	**9/0.131**	**Ours**
In_2S_3	CVD	~ 10	137	7.74×10^{10}	ND	6/8	5
In_2S_3	HT	~ 5	ND	ND	16	2000/100	6
CdTe	CVD	5-11	$0.6*10^{-3}$	10^9	27	18.4/14.7	7
SnTe	PVD	~ 30	71	ND	~ 2	210/730	8
PbS	HT	~ 1	0.472	ND	100	ND	9
PbS	CVD	2-2.6	1621	10^{11}	~ 2	300/300	10
$Pb_{1-x}Sn_xSe$	CVD	~ 15	5.95	ND	~ 3	900/740	11
Te	CVD	6-10	160	ND	~3	4400/2800	12
Commercial Si	ND	ND	0.5	3×10^{12}	ND	ND	13

Ref.: reference. CVD: chemical vapor deposition. PVE: physical vapor epitaxy. ME: mechanical exfoliation. HT: Hydrothermal. ND: no data. Gr: graphene.

Reference

1. Wang, L.; Jie, J. S.; Shao, Z. B.; Zhang, Q.; Zhang, X. H.; Wang, Y. M.; Sun, Z.; Lee, S. T., MoS2/Si Heterojunction with Vertically Standing Layered Structure for Ultrafast, High-Detectivity, Self-Driven Visible-Near Infrared Photodetectors. *Adv. Funct. Mater.* **2015,** *25* (19), 2910-2919.
2. Zheng, Z. Q.; Zhu, L. F.; Wang, B., In2O3 Nanotower Hydrogen Gas Sensors Based on Both Schottky Junction and Thermoelectronic Emission. *Nanoscale Res. Lett.* **2015,** *10*, 293.
3. Li, B.; Huang, L.; Zhong, M. Z.; Li, Y.; Wang, Y.; Li, J. B.; Wei, Z. M., Direct Vapor Phase Growth and Optoelectronic Application of Large Band Offset SnS2/MoS2 Vertical Bilayer Heterostructures with High Lattice Mismatch. *Adv. Electron. Mater.* **2016,** *2* (11), 1600298.
4. Li, Y. T.; Wang, Y.; Huang, L.; Wang, X. T.; Li, X. Y.; Deng, H. X.; Wei, Z. M.; Li, J. B., Anti-Ambipolar Field-Effect Transistors Based On Few-Layer 2D Transition Metal Dichalcogenides. *ACS Appl. Mater. Interfaces* **2016,** *8* (24), 15574-15581.
5. Huang, W.; Gan, L.; Yang, H.; Zhou, N.; Wang, R.; Wu, W.; Li, H.; Ma, Y.; Zeng, H.; Zhai, T., Controlled Synthesis of Ultrathin 2D β-In_2S_3 with Broadband Photoresponse by Chemical Vapor Deposition. *Adv. Funct. Mater.* **2017**, 1702448.
6. Acharya, S.; Dutta, M.; Sarkar, S.; Basak, D.; Chakraborty, S.; Pradhan, N., Synthesis of Micrometer Length Indium Sulfide Nanosheets and Study of Their Dopant Induced Photoresponse Properties. *Chem. Mater.* **2012,** *24* (10), 1779-1785.
7. Cheng, R.; Wen, Y.; Yin, L.; Wang, F.; Wang, F.; Liu, K.; Shifa, T. A.; Li, J.; Jiang, C.; Wang, Z.; He, J., Ultrathin Single-Crystalline CdTe Nanosheets Realized via Van der Waals Epitaxy. *Adv. Mater.* **2017,** *29* (35), 1703122.
8. Yang, J.; Yu, W.; Pan, Z.; Yu, Q.; Yin, Q.; Guo, L.; Zhao, Y.; Sun, T.; Bao, Q.; Zhang, K., Ultra-Broadband Flexible Photodetector Based on Topological Crystalline Insulator SnTe with High Responsivity. *Small* **2018**, e1802598.
9. Schliehe, C.; Juarez, B. H.; Pelletier, M.; Jander, S.; Greshnykh, D.; Nagel, M.; Meyer, A.; Foerster, S.; Kornowski, A.; Klinke, C., Ultrathin PbS Sheets by Two-dimensional Oriented Attachment. *Science* **2010,** *329* (5991), 550-553.
10. Wen, Y.; Wang, Q.; Yin, L.; Liu, Q.; Wang, F.; Wang, F.; Wang, Z.; Liu, K.; Xu, K.; Huang, Y.; Shifa, T. A.; Jiang, C.; Xiong, J.; He, J., Epitaxial 2D PbS Nanoplates Arrays with Highly Efficient Infrared Response. *Adv. Mater.* **2016,** *28* (36), 8051-8057.
11. Wang, Q.; Xu, K.; Wang, Z.; Wang, F.; Huang, Y.; Safdar, M.; Zhan, X.; Wang, F.; Cheng, Z.; He, J., Van Der Waals Epitaxial Ultrathin Two-dimensional Nonlayered Semiconductor for Highly Efficient Flexible Optoelectronic Devices. *Nano Lett.* **2015,** *15* (2), 1183-1189.
12. Wang, Q.; Safdar, M.; Xu, K.; Mirza, M.; Wang, Z.; He, J., Van der Waals Epitaxy and Photoresponse of Hexagonal Tellurium Nanoplates on Flexible Mica Sheets. *ACS Nano* **2014,** *8* (7), 7497-7505.
13. Saran, R.; Curry, R. J., Lead Sulphide Nanocrystal Photodetector Technologies. *Nat. Photonics* **2016,** *10* (2), 81-92.